The Antares neutrino telescope : performance studies and analysis of first data

Bruijn, R.

Publication date
2008

Chapter 2

The Antares neutrino telescope

Neutrino astronomy is dictated by the small interaction cross section of neutrinos and the expected fluxes. On the one hand, the weakly interacting nature of neutrinos makes them excellent probes of distant astrophysical processes. As they are not deflected by magnetic fields they point straight back to their origin, while they have a low probability of being absorbed on their way to Earth. On the other hand, their small interaction probability combined with the expected fluxes require the use of very large detectors and long operation times. To enable the building of a large volume detector, naturally abundant sea-water can be used to detect the luminous interaction products of neutrinos. The neutrino telescope, which is under construction by the Antares collaboration, is based on this principle. In this chapter the Antares neutrino telescope will be presented. The software that is used to simulate both the physics processes that lead to a detectable signal and the detector response to this signal will be described.

2.1 Neutrino interactions

For a neutrino to be detected, it has to produce a detectable signal. Neutrinos interact with matter through the weak force which can be classified in two types. These are the neutral current (NC) interaction, which involves the exchange of a Z boson, or the charged current (CC) interaction, which involves the exchange of a W^+ or W^- boson [32]. These two interaction types can be formulated as

$$\nu_l(\bar{\nu}_l) + N \rightarrow \nu_l(\bar{\nu}_l) + X \ (NC) \tag{2.1}$$

$$\nu_l(\bar{\nu}_l) + N \rightarrow l^-(l^+) + X \ (CC) \tag{2.2}$$

Where $\nu_l(\bar{\nu}_l)$ is the (anti-)neutrino of type l, N the target nucleon, X the hadronic interaction products and l the lepton. At the energies considered in this work, the interaction cross section is predominantly inelastic. The involved lepton flavor can be one of the three types: electron (e), muon (μ) or tau (τ). The cross sections of the charged-current interactions involving muon (anti-) neutrinos are

shown in figure 2.1 as function of neutrino energy. The small values of the cross sections motivate the need for a large interaction volume. The charged particles originating from a neutrino interaction can produce a detectable signal (see section 2.4).

2.2 Detection principle

The Antares neutrino telescope consists of a three-dimensional array of light-sensitive photo-multiplier tubes (PMTs) installed at a large depth in the Mediterranean sea. This array of PMTs can detect photons produced by relativistic charged particles emerging from neutrino interactions in the sea-water or in the rock below the detector.

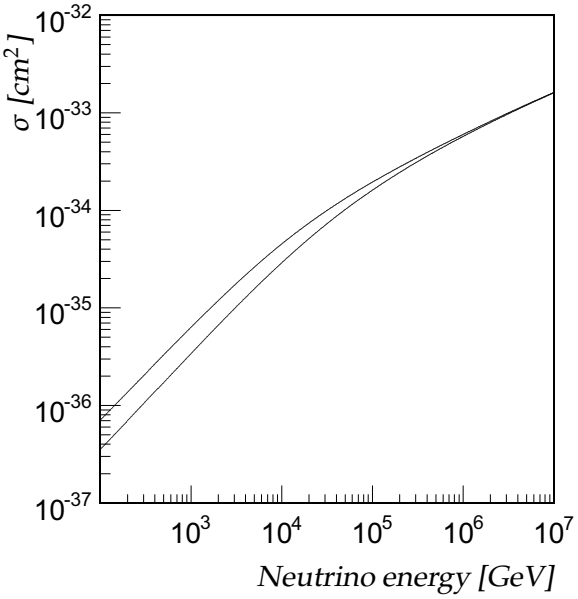

Figure 2.1: *Muon neutrino (top line) and anti-neutrino (bottom line) charged-current cross sections as function of energy, obtained using the CTEQ6D [33] quark density distributions.*

The main experimental signature for the Antares neutrino telescope is the signal produced by muons created in the charged-current interaction of muon-neutrinos. A relativistic muon propagating through the sea water emits Cherenkov light (section 2.4) that can be detected by the PMTs. The muons can travel large distances. In water, a 10 GeV muon can travel several tens of meters before it stops, while a 10^7 GeV muon can traverse some tens of kilometers [14]. The muon created in a muon-neutrino interaction retains the direction of the neutrino to a large extent. This can be expressed as the angle between the incident neutrino and the outgoing muon ($\theta_{\nu-\mu}$). The upper limit on this angle can be approximated by

$$\langle \theta_{\nu-\mu} \rangle \leq \frac{1.5^\circ}{\sqrt{E_\nu [TeV]}} \tag{2.3}$$

where E_ν is the neutrino energy. A muon traveling through rock or water is subject to multiple scattering. The deviation of the muon direction due to this

process (θ_{ms}) after traveling a distance x is given by [14] :

$$\theta_{ms} = \frac{13.6MeV}{E_\mu}\sqrt{x/X_0}\,[1 + 0.0038\ln(x/X_0)] \tag{2.4}$$

where X_0 is the radiation length of the medium. At the energies and distances considered in this work, θ_{ms} is smaller than $\theta_{\nu-\mu}$. The relation between the neutrino and muon directions is essential for the concept of a neutrino telescope. When the direction of the muon can be determined, so can the direction of the incident neutrino. As neutrinos are not deflected by (extra-)galactic magnetic fields, it is possible to trace the muon back to the origin of the neutrino. This is equivalent to optical astronomy where photons point back to their source. In this work, a technique is developed to derive the muon direction from the observed photons. This process is commonly referred to as muon track reconstruction.

2.3 Other signals

The momentum transferred to the hadronic products in the neutrino interaction is in general such that the charged particles also produce a detectable signal. While propagating through the sea water, they can interact with other nuclei and produce additional hadrons which in turn can produce a detectable signal and interact, thus forming a so-called hadronic shower. The decay of neutral pions introduces an electro-magnetic component to the shower. The hadronic cascades continue until all energy has been dissipated. For a nuclear interaction length of about 80 cm, the extension of such a shower in water is limited to several meters. Electrons produced in a charged-current interaction of an electron-neutrino radiate photons through Bremsstrahlung which in turn can be converted to electron-positron pairs. The electrons and positrons undergo Bremsstrahlung. The typical distance between interactions is given by the radiation length. The formed electro-magnetic cascades also have a limited size due to the limited radiation length of water of 36 cm. Therefore neutral-current neutrino interactions and charged-current electron-neutrino interactions should occur close to or within the detector volume to be detectable. When this happens, the detected light can be used to infer properties of the interacting neutrino [34]. The tau-lepton, which can be created in a charged-current interaction of a tau-neutrino, has a lifetime much shorter than that of the muon ($2.91 \cdot 10^{-13}$ seconds compared to $2.19 \cdot 10^{-6}$ seconds). In addition to the shower at the interaction point, a shower can occur when the tau decays. At sufficiently high energies, the tau-lepton can traverse a noticeable distance. Some fraction of the tau-lepton decays produce a muon (17.8%), which can mimic the interaction of a muon neutrino.

2.4 Cherenkov light

The detection of neutrinos happens indirectly through their interaction products. A charged particle traveling through a medium at a velocity exceeding the speed of light in the medium emits Cherenkov radiation [35]. This electro-magnetic radiation is emitted at a characteristic angle θ_c with respect to the direction of the charged particle, thus forming a conical light-front (figure 2.2). The angle θ_c can be expressed as

$$\cos(\theta_c) = 1/\beta n \tag{2.5}$$

where β is the ratio of the velocity of the particle (v) to the speed of light (c) and n is the index of refraction for the medium. At the location of the Antares neutrino telescope, the value of n is about 1.35 [36]. Thus, for relativistic particles ($\beta \approx 1$) the value of θ_c is about 42.2°. The number of Cherenkov photons emitted by a particle with unit charge (e.g. a muon) per unit wavelength ($\delta\lambda$) and per unit track length (δx) is given by

$$\frac{dN}{dxd\lambda} = 2\pi\alpha\frac{1}{\lambda^2}\left(1 - \frac{1}{\beta^2 n^2}\right) \tag{2.6}$$

where λ is the wavelength of the emitted photon and α the fine-structure constant. Considering the typical efficiency of a PMT (300 - 600 nm), the detectable photons emitted per meter number about 35000.

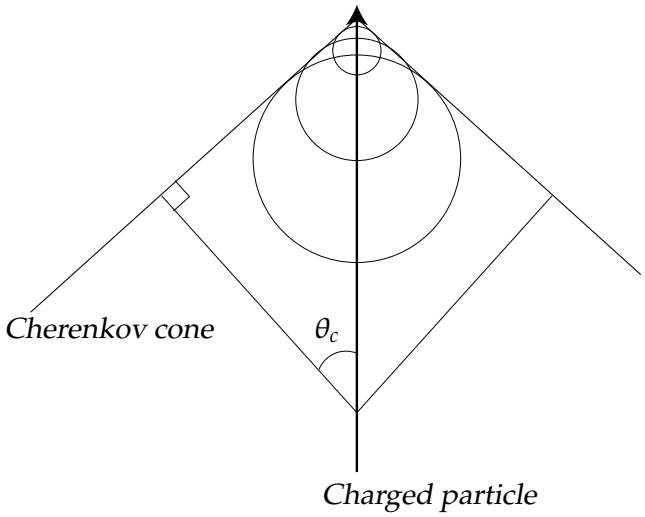

Figure 2.2: *Schematic view of the production of Cherenkov light by a charged particle. According to the principle of Huygens, spherical light waves are produced along the particle trajectory. The light waves interfere because the particle moves faster through the water than the light. As a result a sharp wave front is formed that can be detected with the PMTs.*

Photons traveling through the water are subject to several processes. They can be absorbed and scattered by molecules and particles in the water. Absorption of photons results in an attenuation of the intensity of the light emitted by a source

at a given distance. Scattering of photons affects the original angular distribution of the emitted photons. With increasing distance, the correlation between the angular distribution of the photons and the source position deteriorates. The effects of photon absorption and scattering can be quantified by the absorption length (λ_{abs}) and the scattering length (λ_{scat}) which are both wavelength dependent. The intensity of the light emitted by a muon (I_0) is related to the intensity (I) at distance r from the muon track by

$$I \propto I_0 \frac{1}{r} e^{\frac{-r}{\lambda_{abs}}} \tag{2.7}$$

The factor $1/r$ comes from the geometrical spread of the Cherenkov cone. The scattering length λ_{scat} is the length at which on average a fraction of e^{-1} of the photons is unscattered. In situ measurements of the water properties [37] give values for λ_{abs} and λ_{scat} of about 60 and 260 meters respectively, at a photon wavelength of 473 nm. The group velocity of light in water is relevant for the measured arrival times of the photons [38]. The corresponding index of refraction has been measured and found to be 1.38 [39] for a wavelength of 460 nm. In the simulation and muon track reconstruction, the assumed wavelength of the photons is 460 nm. Dispersion due to the wavelength dependence of the refractive index introduces a delay of up to 2 ns of the arrival time of photons at a distance of 300 meters [39]. This is included in the simulation.

2.5 Muon energy loss

A muon can interact with matter through several processes [14]. When a muon passes through matter, it ionizes or excites the surrounding atoms, transferring in each case a small a mount of energy. A muon can also interact with atoms through radiative processes. In the nuclear electric field of an atom, a muon can radiate a photon. This process is referred to as Bremsstrahlung. When an electron-positron pair is created, the process is referred to as pair-production. A muon can also interact with an atomic nucleus by the exchange of a (virtual) photon. The relative importance of these processes depends on the energy of the muon, and is summarized in figure 2.3. Below approximately 1 TeV, the energy loss is dominated by the ionisation process. Energy loss through ionisation is approximately constant at a level of about 0.2 GeV/m. The radiative processes have an approximately linear dependence on the energy of the muon. Above about 1 TeV, radiative processes dominate the total energy loss. Because of the stochastic nature of the radiative processes, the actual energy loss shows large fluctuations. The fluctuations manifest themselves by electro-magnetic (pair-production and Bremsstrahlung) or hadronic (photo-nuclear) showers. The cross sections of the radiative processes can be expressed as function of the fractional energy loss ν. The cross section for Bremsstrahlung scales with $1/\nu$ while the dependence of

the pair-production cross section varies between ν^{-2} and ν^{-3}. So, hard energy losses are more likely to happen with Bremsstrahlung showers. Particle showers occurring along a muon track show a particular signature in the detector which have to be taken care of when reconstructing muon tracks. The effects of these showers on the muon track reconstruction and further analyses are considered in chapters 3 and 4.

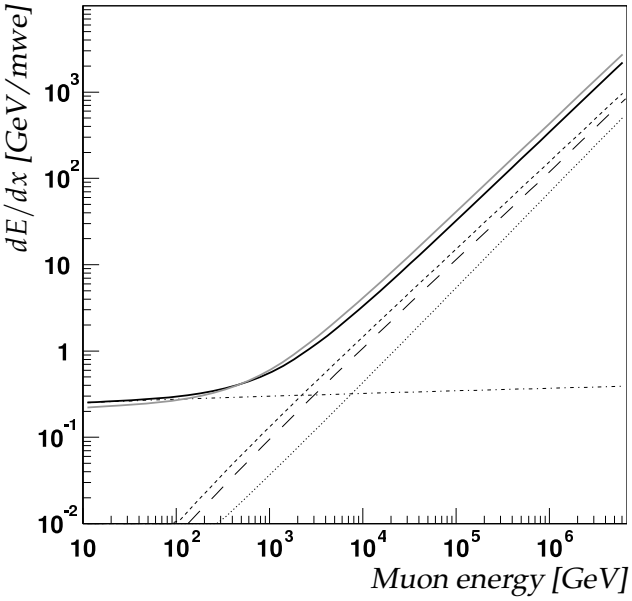

Figure 2.3: *Muon energy loss in GeV per meter water equivalent in water (solid black line) and rock (solid grey line). The separate contributions to the energy loss in water are indicated by the other line types. The short dashed line indicates pair production, the long dashed line Bremsstrahlung, the dotted line nuclear interactions and the dash-dotted line ionisation losses.*

2.6 The Antares neutrino telescope

This section describes the detector hardware design and the read-out system. The telescope is located in the Mediterranean Sea at a depth of 2.475 km at 42°50′ N, 6°10′ E, which is approximately 40 km out of the coast from the city of Toulon, France.

2.6.1 Optical module

The basic light-sensitive element of the Antares detector is a photo-multiplier tube of the type Hamamatsu R7081-20 [40]. It is a hemispherical PMT of 10″ in diameter and has a total sensitive area of about 500 cm^2. The number of amplification stages is 14 and the nominal gain is $5 \cdot 10^7$ at a high voltage of 1760 V. This PMT is sensitive to single photons in the wavelength range between 300 and 600 nm. It has a peak quantum efficiency of about 25 % between 350 and 450 nm. The determination of muon track parameters relies on an accurate measurement of the times at which photons arrive at the PMT. The transit time is the time

between the illumination of the photo-cathode and a subsequent current pulse on the anode. The transit time spread (TTS) is a measure of the fluctuations in transit time in response to single photons. The TTS is defined as the full-width-at-half-maximum (FWHM) of the probability distribution of these fluctuations. The transit time depends on several parameters. Among these parameters are the position and angle of illumination, high-voltage and the intensity of the light. In general the transit time spread is proportional to $1/\sqrt{a_i}$ [41] where a_i is the number of photons. The measurement of the number of photons is usually referred to as the amplitude. The single photon TTS of the PMT is 2.6 ns FWHM. The charge resolution is about 30 % [40]. Every PMT is mounted in a pressure resistant glass sphere with a diameter of 43 cm and a thickness of 15 mm. A gel provides optical and mechanical contact between the PMT and the inner sphere. Shielding from the Earth magnetic field is provided by a μ-metal cage which surrounds the PMT and is partly embedded in the gel. Power to the PMT is supplied by means of an electronics board mounted on the socket of the PMT. This board also transmits the output from the anode and last dynode of the tube. To calibrate the PMT, in particular the transit time, a blue (470 nm) light emitting diode (LED) is attached to the back of the PMT. The back hemisphere of the glass sphere is made opaque by covering it with black paint. A penetrator is used for a cable carrying wires for power, readout and control. The total setup is referred to as an Optical Module (OM). A schematic drawing is shown in figure 2.4.

As the optical modules are the light measuring devices in Antares, it is important to quantify their sensitivity. The limited size of the PMT implies that the optical modules have a varying directional sensitivity. Photons arriving head-on, have a high probability of being detected. On the other side, photons arriving from the rear, hitting the black surface, will not induce a signal. The angular distribution of photons from the different sources covers the complete 4π solid angle. The probability of a photon to be detected depends on several parameters. In addition to the quantum efficiency of the PMT and the absorption coefficients of the gel and glass, the exact path a photon follows through the optical module is of influence. The incident angles and refractive indices determine which path a photon will travel through different materials. Photons arriving at backward angles can be refracted onto the photo-cathode. In order to quantify the angular acceptance of the optical module, measurements and studies have been done. Figure 2.5 shows the relative angular acceptance determined from measurements using atmospheric muons [40] and with a ray-tracing simulation [42]. Also shown is a parameterisation which was based on measurements on a obsolete configuration of the optical module. This parameterisation was used in older versions of the Antares simulation software. As can be seen from figure 2.5, there is an uncertainty in the angular acceptance for the backward regions. This uncertainty will induce a systematic error in the measurements. Currently, new measurements are done in order to reduce this error.

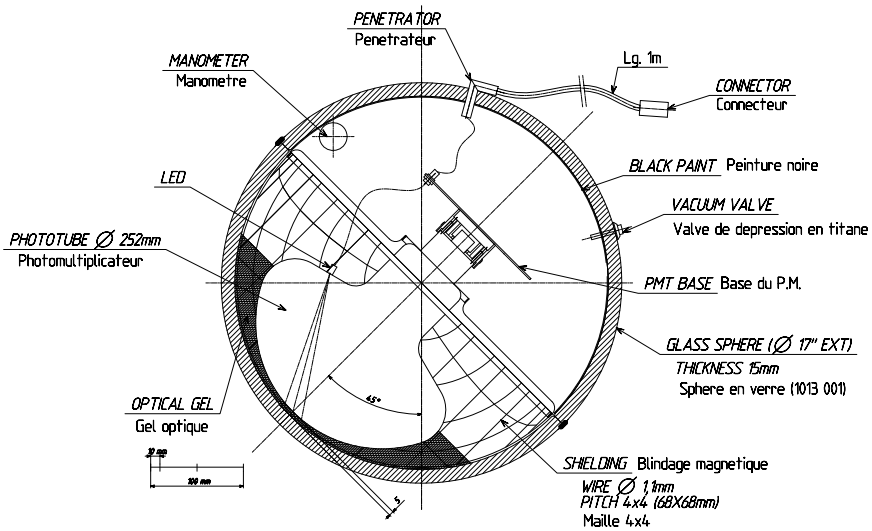

Figure 2.4: *Schematic cross section of the optical module used in the Antares detector.*

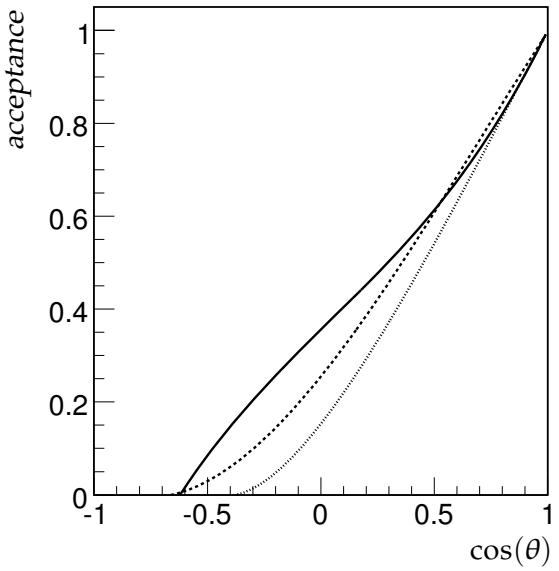

Figure 2.5: *Relative angular acceptance of the Antares optical module as function of the incident angle of the photon (θ). The angle θ is defined with respect to the axis of the PMT and $\cos(\theta) = 1$ corresponds to photons hitting the photo-cathode of the PMT head-on. The solid line is obtained from a ray-tracing simulation [42] and the dashed line from measurements using atmospheric muons [40]. The dotted line was used in older versions of the Antares simulation software.*

2.6.2 Detector layout

The detector layout has been optimized such that the optical modules are distributed in a large (effective) volume and the transport of data, power and control signals is possible. It incorporates equipment for calibration and monitoring of the detector and the environment. An overview of the detector geometry is shown in figure 2.6. Three optical modules are mounted on a titanium frame,

called the optical module frame (OMF), as shown in figure 2.7. The optical modules point downwards at an angle of 45° from vertical, and 120° away from each other. Several other components are mounted on the OMF. A titanium cylinder is used to house the electronics for the read-out of the optical modules and various other instruments for calibration and monitoring. This cylinder is referred to as the local control module (LCM). Some instruments used for calibration of the detector are mounted on some OMFs. A pressure-resistant glass cylinder containing an array of LEDs is used as an optical beacon. These optical beacons are distributed in the detector and are used for the calibration of the PMTs (see section 2.6.4). The OMF with all its components is referred to as a storey. The storeys are linked by an electro-mechanical cable, which has sufficient tensile strength and contains all necessary cables for power and optical fibers for data transport. Five storeys make up a sector. Every sector has its own power supply and communication channel to shore. One of the five storeys in a sector has the functionality in distributing control and data signals to shore. This functionality is implemented in the electronics container. This local control module is referred to as the master local control module (MLCM). Five sectors, thus 25 storeys, are organized in a single vertical line. The storeys are separated by 14.5 meters. The first storey is at about 100 meters from the sea-bottom. A buoyant element at the top keeps the line vertical. A bottom string socket (BSS) is located at the bottom of the line. The BSS consists of a dead-weight to anchor the line to the sea-bottom and a titanium container. This container houses the string control module (SCM) and the string power module (SPM). The SCM consists of electronics for the read-out of several instruments and the distribution of a common clock signal. In addition, the signals from the different sectors are merged into a single communication channel. The SPM distributes power to the different sectors of the line. A laser beacon is mounted on two of the BSSs which is used as an alternative optical beacon (see section 2.6.4). The detector consists of 12 lines, making a total of 900 PMTs. The relative positions of the 12 lines on the sea-floor is shown in figure 2.8. The lines are connected via an interconnecting link cable to a central junction box. The junction box forms the distribution point of power, clock and signals from the shore to the lines. The junction box is connected to shore through a 40 km long main electro-optical cable. The on-shore part of the detector consists of a power feed station and a shore station, where data are received and filtered, a common clock signal is generated and the detector control is housed. The shore station is located in the town of La Seyne-sur-Mer. A dedicated line for the monitoring of the environment is placed in the vicinity of the detector. The detector is installed line by line. Each line is lowered from a ship. A remotely operated submarine vehicle (ROV) is used to connect the line to the junction box with an interconnecting link cable.

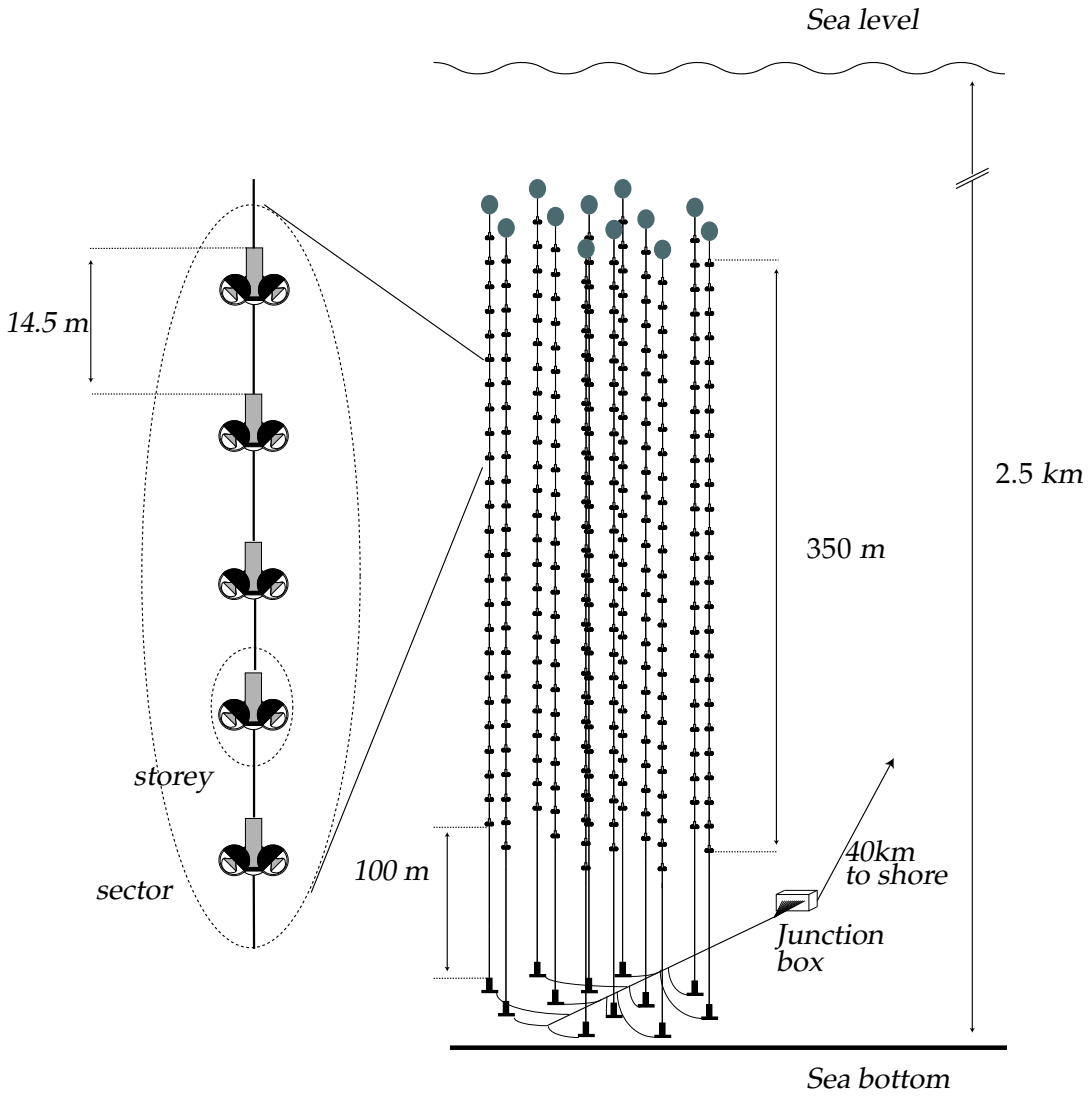

Figure 2.6: *Schematic drawing of the Antares neutrino telescope. The drawing shows the 12 detector lines and one sector consisting of 5 storeys. Each storey has 3 optical modules. The junction box connects the 12 lines to shore through a 40 km long cable.*

2.6.3 Data acquisition

The data acquisition (DAQ) system [44] of the Antares detector includes the digitization of the analogue signal from the PMTs, the transport of the data to shore and the subsequent filtering and storage of the data. The DAQ system is designed around the *all-data-to-shore* concept, which entails the bias-free transport of all photon signals recorded by the optical modules to the shore station where

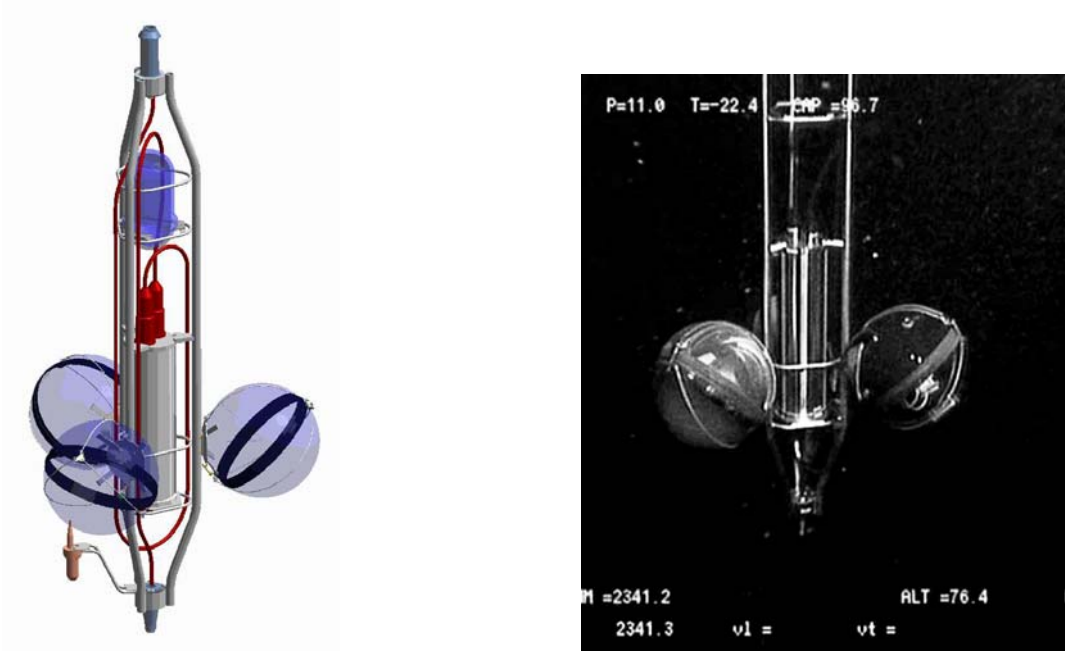

Figure 2.7: *Left : A storey contains three optical modules, a container housing the electronics, and optical beacon and an acoustic transceiver. Right : Photograph of a storey in situ [43].*

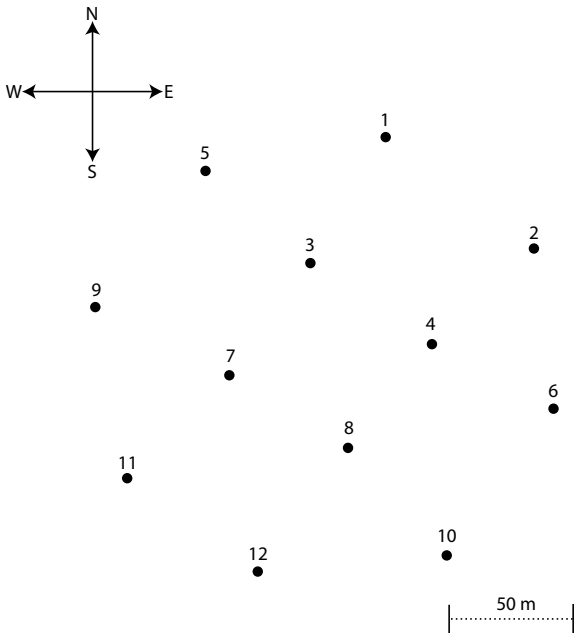

Figure 2.8: *Schematic view of the floor layout of the lines. The numbering scheme of the detector lines is also indicated.*

filtering is performed. A schematic overview of the DAQ system is shown in figure 2.9. The signal from a PMT is read-out and digitized by a custom front-end chip: the analogue ring sampler, ARS [45]. When the signal at the anode of the PMT exceeds a threshold voltage, the charge is integrated by the ARS. The typical threshold value corresponds to 0.3 photo-electrons. The duration of the integration gate is set to 33 ns. The ARS can also function in waveform mode, in which the photo-multiplier signal is sampled and digitized. In this work, the waveform mode is not used. A local clock supplies a reference signal to the ARS which is used to timestamp each PMT signal above threshold. The clock has a frequency of 20 MHz. Sub-nanosecond timing is achieved by time-to-voltage converters (TVCs) which provide interpolation between the clock pulses and are read-out by 8-bit analog-to-digital converters (ADCs). The combined time and charge information of a PMT signal is referred to as a hit. After the integration gate, the ARS has a dead-time of about 200 ns. In order to reduce the effects of the dead-time, each PMT is read-out by two ARS chips. Each pair of ARS chips functions in a token ring scheme. The minimum time between two consecutive hits is 45 ns. The ARS is read-out by a field programmable gate array (FPGA) and buffered in a 64 MB memory. The data are organized in frames covering a time period of 104.858 ms. A central processing unit (CPU), running the VxWorks real time operating system functions as the interface with the on-shore systems. The CPU runs two programs. The first is used for the processing of ARS data (*DAQHarness*). The second program (*SCHarness*) is used to control several devices which are connected via a serial port to the CPU, such as the power supply, compass and tilt-meter. Data from these devices are referred to as slow-control data. The communication to shore is done using the TCP/IP protocol. For this, the CPU has a 100 Mb/s Ethernet interface. The effective throughput of the CPU corresponds to a maximum mean rate of about 300 kHz per optical module. The data are transmitted using optical fibers. The additional functionality of the MLCM consists of merging the bi-directional optical 100 Mb/s Ethernet links from the LCMs into a single 1 Gb/s Ethernet link to shore using two uni-directional optical fibers, one for incoming and one for outgoing data. In the SCM, the signals from the MLCMs are combined in a single pair of optical fibers. The pairs are then routed through the junction box to the shore station.

On shore, the optical signals are decoded and routed through a large 1 Gb/s Ethernet switch. This Ethernet switch connects the off-shore processors to the on-shore computing farm, consisting of commodity PCs. By the use of Ethernet and the TCP/IP protocol, each on- and off-shore processor is addressable by its IP-address. The transfer of data and control signal is thus completely transparent.

The software processes running on- and off-shore are synchronised by an implementation of a finite state machine using the CHSM language [46]. The program *RunControl* [47] manages the state-transitions of the processes and distributes configuration data. All configuration data are stored in a database. The *RunControl* is the main user-interface to the experiment. Data and messages are

distributed following the concept of tagged data by the *Ligier* program, which is an implementation of the *ControlHost* [48] package. The data-taking is organized in data-taking runs. Each data-taking run corresponds to a period of typically 5 hours. The start and stop times of each run are stored in a database by the Run-Control. During a run, the data frames from the LCMs corresponding to the same time period are sent to a single on-shore PC. The frames of a following time period are then sent to a different PC. The set of frames of a single time period are referred to as a timeslice.

When required, the DAQ system can run with a sampling factor. This reduces the incoming data-stream by synchronously processing only every N^{th} timeslice. This reduction already takes place at the level of the (M)LCM where only the N^{th} frame is written to the on-board memory.

Following the all-data-to-shore principle, no filtering of the data, except for a 0.3 photo-electron threshold, is done off-shore. Consequently, a large amount of data (see section 2.7) has to be processed in real-time. This processing is done using the farm of PCs. Each of these PCs have the *DataFilter* program running for this task. The method of extracting the physics signal from the data is described in section 2.8. After filtering, the selected data are sent to a PC running the *DataWriter* program which writes the data to disk. For the storage of data, the ROOT [49] software package is used. Slow-control data-taking is controlled by the *ScDataPolling* program and written to the database by the *DBWriter* program.

Clock

The clocks in the (M)LCMs are synchronised by a common clock signal. This clock signal is generated on-shore and is synchronised with GPS time to an accuracy of 100 ns. The clock signal is converted into an optical signal and distributed through the optical network. By measuring the return time of a calibration signal, the relative phase-offsets of the local clocks can be determined.

2.6.4 Calibration

Position calibration

The Antares detector is not a rigid structure, and the deep-sea environmental conditions are variable. The detector lines are subject to forces caused by sea currents, which make them sway and torque. For the reconstruction it is necessary to determine the relative position of the PMTs. For this, two independent systems are in place [1]. The first is the acoustic positioning system. By measuring the travel times of acoustic pulses, a three-dimensional reconstruction of the detector elements can be made. The pulses are in the 40-60 kHz range and are transmitted by emitters located at the BSS of each line. Along each line, there are

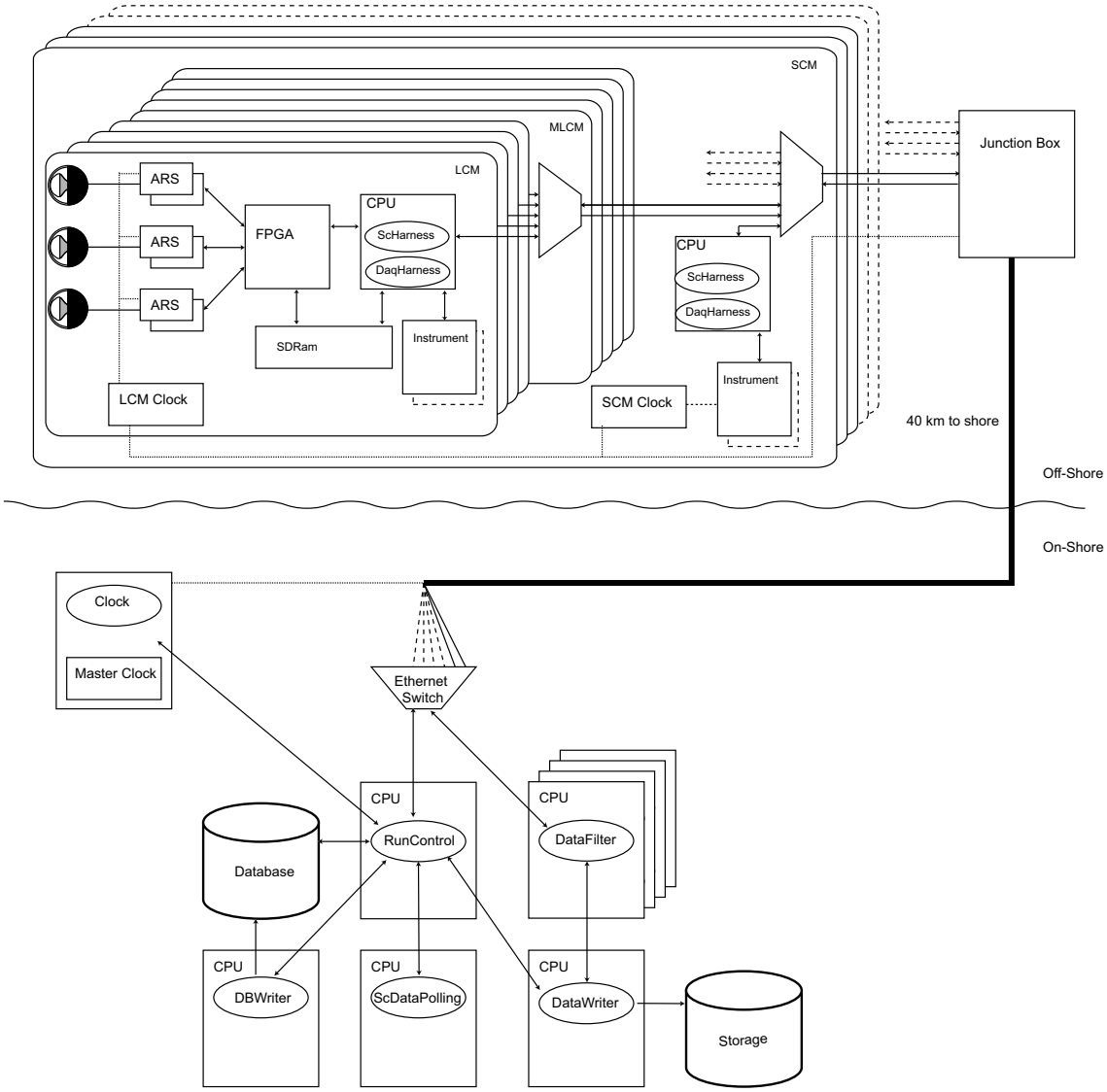

Figure 2.9: *Schematic overview of the Antares DAQ system. Square boxes indicate hardware components and ovals indicate software processes. Lines with arrows indicate the direction of data flow. The dotted line indicates the distribution of the clock signal. The thick black line indicates the 40 km long main electro-optical cable. Cylinders indicate data storage systems.*

five acoustic receivers, called hydrophones. The transmitters are also capable of receiving signals. Four additional autonomous transponders are located around the detector to increase the accuracy of the global alignment. The depth of the BSS is determined with pressure sensors located at the BSS and during connection to the junction box with a pressure sensor on the submarine. The speed of

sound is dependent on pressure, temperature and salinity. Therefore, the detector is equipped with sound velocity meters and with independent pressure, temperature and salinity measuring devices. In addition to the acoustic system, each LCM is equipped with a bi-axial tilt meter and compass. This is used to measure pitch, roll and heading. The positioning system is designed to measure the position of each OM within 10-20 cm [1]. The absolute orientation of the detector is determined with the use of the autonomous transponders, which have a known position, determined during their deployment. The relevant variables are the tilt angles along the North-South and East-West axes and the heading with respect to the North-South axis.

Time calibration

The time resolution of the Antares detector is limited by the PMT transit time spread (see section 2.6.1) and the scattering and chromatic dispersion of Cherenkov light (see section 2.4). The electronics of the Antares telescope is designed to contribute no more than 0.5 ns to the uncertainty in the timing. Thus, the timing calibration should have a precision better than a nanosecond. Several systems are in place to perform calibration measurements. As mentioned in section 2.6.3, the LCMs can echo a calibration pulse sent by the clock system. In this way, the relative offsets of the local clocks can be measured with 0.1 ns accuracy. The internal LED of the OMs (section 2.6.1) is used to measure the relative variation of the TTS of the PMTs. For the measurement of the relative timing between different optical modules and the influence of light propagation, a system of optical beacons is in place [50]. The system consists of two types of pulsed light sources.

First, there are LED beacons mounted on several storeys on a line that can illuminate storeys on neighboring lines. A LED beacon consists of a borosilicate glass cylinder containing a hexagonal structure with on each face 6 LEDs. One of the LEDs on each face points upwards. These LEDs illuminate the storeys above on the same line. The LEDs emit light with a wavelength of 472 nm. The rise time of the light pulse is about 2 ns. The LEDs flash at a typical frequency of a few Hz.

Second, a laser beacon is mounted at the bottom of two lines. The laser beacons illuminate the lower part of the detector. The laser beacon is housed in a cylindrical container. The light is emitted from the top through a diffuser. The laser emits light at a wavelength of 532 nm in a triggered mode.

Tests with the optical beacon system [50] have shown that the timing resolution of the detector electronics is about 0.5 ns, well within the design parameters.

2.7 Signal and background

Although the main aim of the Antares telescope is to detect light caused by the interactions of cosmic neutrinos, it is by far not the only source of light in the

deep-sea. Three sources of detectable light are shown schematically in figure 2.10. Particles, known as cosmic rays, impinging on the atmosphere, can interact and iniate particle cascades, producing air-showers. Charged mesons created in these showers can decay to muons and neutrinos. A fraction of the muons created in the showers overhead can reach the detector site despite its depth. Several muons originating from a single cosmic-ray interaction in the atmosphere can reach the detector simultaneously. Due to the mass column presented by the Earth, the angular distribution of the atmospheric muons is limited to the downward directions. Neutrinos produced by cosmic-ray interactions, however, can traverse the Earth. These neutrinos can interact in the vicinity of the detector and produce a muon or other detectable particles. Muons created in the interactions of atmospheric neutrinos can originate from all directions. The muon fluxes caused by atmospheric neutrinos and atmospheric muons are shown in figure 2.11. Around horizontal directions, the flux of atmospheric neutrinos is enhanced due to the increased path length in the upper atmosphere, favoring the decay of mesons. The signals caused by muons originating from any of the three sources mentioned above are indistinguishable. After muon track reconstruction, the different signals can be distinguished. By selecting tracks with upward going directions, the atmospheric muon bundles can be rejected. However, atmospheric muons can sometimes be mis-reconstructed and classified as upward going. Hence, when looking for cosmic neutrinos, there is a background from both atmospheric muons and neutrinos. Various ways to reduce this background are presented in chapter 5.

Another kind of background that is not related to a passing muon or a neutrino interaction is present in the deep-sea. This background can be expressed as the number of detected photons per optical module per second. A large contribution to this background is due to the decay of ^{40}K. The dominating decay channel is a β decay producing a low-energy (up to 1.3 MeV) electron which then emits Cherenkov light. The contribution to the background depends on the concentration of ^{40}K and the absorption length. The counting rate has been estimated and found to be about 30 kHz [51],[52] and [53]. Another contribution to the counting rate is caused by light emitted by various living organisms in the deep-sea. This is known as bioluminescence [54],[55]. The variation of the counting rate due to bioluminescence shows a few different time scales [53]. A continuous component can be recognized to which the potassium decay, the PMT dark current (about 3 kHz) and bioluminescent bacteria contribute. This contribution is referred to as the baseline rate. It can vary on a timescale of several hours to days between about 50 kHz and several hundred kHz. On top of the baseline rate, bursts of bioluminescent activity occur, lasting from several milliseconds to minutes. These bursts are very local, with counting rates varying from hundreds of kHz to a MHz. These bursts are attributed to macro-organisms. The number of bursts is quantified by the burstfraction, which is the fraction of time that the counting rate exceeds the baseline by 20 % or more.

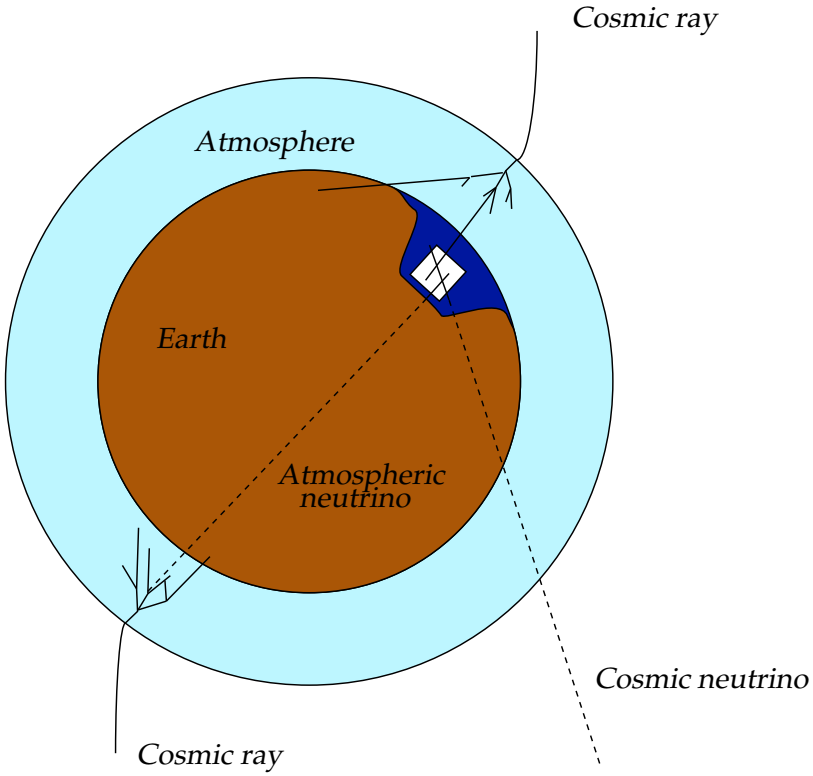

Figure 2.10: *Schematic drawing of the different sources of muons seen in the detector. A cosmic neutrino (dashed, lower right) crosses the Earth and interacts near the detector, creating a detectable muon. A cosmic ray induced muon can reach the detector. A cosmic-ray induced neutrino can cross the Earth and produce a detectable muon as well.*

The background is handled at several levels. The incoming signal of the detector is filtered. In this, the correlated signals expected from muons are separated from the uncorrelated signals of the background. This filtering is described in section 2.8. The influence of the background rate on the determination of muon track parameters is described in chapters 3 and 5. The final background rejection is discussed in chapter 5.

2.8 Trigger

All PMT signals exceeding the 0.3 photo-electron threshold are transferred to shore. These hits are referred to as *L0* hits. The dominant contribution to the data are the hits due to the decay of ^{40}K and bioluminescence. At a rate of 70 kHz per optical module, this results in about 0.5 GB/s transferred to shore. The hits

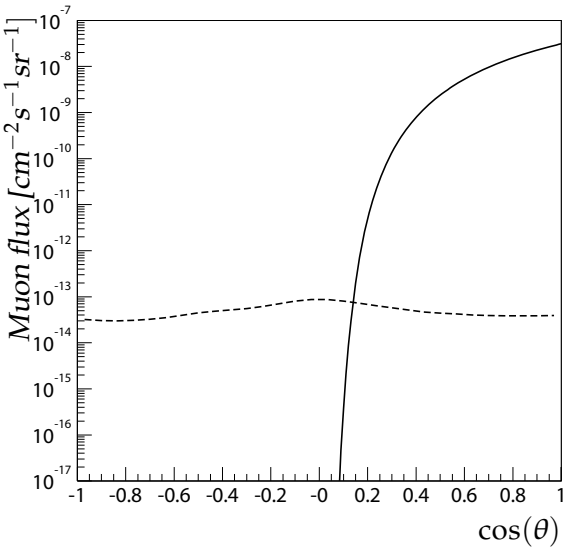

Figure 2.11: *Muon flux at a depth of 2.1 km as a function of zenith angle. The zenith angle indicates the direction from where the muons are coming,* $\cos(\theta) = 1$ *indicates from above the detector. The solid line corresponds to the flux of atmospheric muons. The dashed line corresponds to the flux of muons due to atmospheric neutrinos. Only muons with an energy larger than 100 GeV are included.*

caused by this background are uncorrelated and so constitute a random background. The photons which originate from a single event, e.g. a particle crossing the detector, are causally related. A recorded hit from such an event therefore provides information on possible times and positions of other photons that can be detected. The causal relations can thus be used to filter the data. In general, this is done by finding clusters of correlated hits. A cluster of correlated hits is defined as a set of hits, which are all pair-wise related through a causality criterion. When a sufficiently large cluster of causally related hits in a timeslice is found, the data are saved, otherwise they are discarded. The set of correlated hits is usually referred to as an event. The data contain all hits that triggered the event, together with all hits in a time window from 2 μs before the first hit to 2 μs after the last hit (the so-called snapshot). The event is stored in a data structure called *PhysicsEvent*. The process of finding the event is done in software that runs on the PCs receiving the timeslices. Each of these PCs run the DataFilter program. As all the triggering is done in software there is a large flexibility in the algorithms used to filter the data. Different trigger algorithms can be used for different analyses. Several trigger algorithms can run in parallel on the same data.

In the following, the main trigger algorithm will be described. The trigger exploits the causal relation between hits caused by a relativistic muon crossing the detector. As a first step, the trigger algorithm searches for hits which form a coincidence within a storey, or alternatively single PMT's with a large amplitude. The time window for coincidence is $\pm$20 ns. The selected hits are called *L1* hits. The selection of L1 hits is made to suppress random background. Multiple photons arriving on the same PMT within the integration gate of the ARS will increase the measured charge. The time window of 20 ns accounts for time delays due to the difference in position of the PMTs, dispersion and scattering of the light and uncertainties, at triggering time, in time calibration. The threshold for

a high-amplitude L1 hit is set at 2.5 photo-electrons. Considering muons travel at the speed of light, the largest time difference between two PMTs is associated with the velocity of photons traveling through the water. This speed is equal to the speed of light divided by the index of refraction. So, for two hits i and j to be causally related

$$|t_i - t_j| \leq |\vec{x}_i - \vec{x}_j| \times n_g/c \tag{2.8}$$

Where $t_{i(j)}$ and $\vec{x}_{i(j)}$ are the time and position, respectively, at which hit $i(j)$ is recorded. The speed of light in vacuum is given by c and the group refractive index by n_g. The trigger algorithm looks for the largest subset of L1 hits which are pair-wise causally related according to equation 2.8. The minimum number of causally related L1 hits required to trigger the event is usually set at 5. The causality relation (2.8) is valid for a muon traveling in any direction. By adding information about the (assumed) direction of the muon, the causality criterium can be made more restrictive. In the context of gamma-ray burst studies [47] a *directional* causality criterium was developed. This causality relation will be described in more detail in chapter 3. The standard trigger uses this directional causality relation to reduce the rate of triggers due to random background. When a sufficient number of causally related hits are found, the algorithm applies the directional causality relation to the hits. This is done for about 200 different directions spread isotropically over the full solid angle. The number of directions matches the field of view of the directional trigger. When for a given direction a sufficiently large cluster of hits is found, the event is written to disk. Besides storing triggered events, all incoming data is summarized. A *SummaryTimeSlice* is generated for each timeslice which contains the number of L0 hits that were recorded by each optical module. The SummaryTimeSlices are stored together with the PhysicsEvents.

Several trigger algorithms can run in parallel. These include a dedicated trigger for gamma-ray bursts [47], a dedicated trigger for magnetic monopoles [56] and a source tracking trigger.

The trigger greatly reduces the data-stream. The trigger rate due to random background depends on the rate per optical module. For background rates of 70, 100 and 200 kHz per optical module the respective trigger rates are about 0.01, 0.1 and 30 Hz, corresponding to data rates between about 0.03 and 180 kB/s. The dominating trigger rate with low background is due to the atmospheric muons passing the detector resulting in a rate of about 3 Hz. At trigger level, no distinction is made between events due to atmospheric muons, atmospheric neutrinos or cosmic neutrinos. Further off-line analyses are necessary for further separation. The first step is the determination of the parameters that describe the muon trajectory.

2.9 Current status

Installation of the Antares neutrino telescope began on February 14^{th} 2006 when the first detector line was deployed. This line was connected to the junction box on March 2^{nd}. The line could be operated immediately and data were taken as of day one. Line 1 operated alone until September 21^{st} 2006, when a second line, Line 2, was connected. A detailed analysis of the data taken with Line 1, is presented in chapter 4. The operation of Line 1 overlapped with the operation of a designated instrumentation line. This line, called the Mini Instrumentation Line with Optical Modules (MILOM), was operational from April 2005. The goal of the MILOM was to check the detector elements and to validate the performance of the calibration devices. The MILOM consisted of three storeys. It was equipped with four optical modules, three on the second storey and a single optical module on the top storey. It contained three optical beacons, two LED beacons on the top and bottom storey and a laser beacon on the BSS. Several devices to measure the water properties were mounted on the MILOM. An acoustic Doppler current profiler (ADCP) was installed on the top storey to measure water currents. A conductivity and temperature sensor was mounted on the first storey and a sound velocity sensor on the second storey. Acoustic hydrophones were mounted on several storeys. Operation of the MILOM validated most of the systems [53]. The timing resolution was found to be better than 0.5 ns and the position resolution about 10 cm. Today (December 2007) the Antares neutrino telescope has ten lines and an instrumentation line operational. The full detector is expected to be operational in the beginning of 2008.

2.10 Simulation

In this section, the software used for the simulation of the processes leading to a detectable signal in the detector and the subsequent detector response are described. This includes neutrino and cosmic ray interactions, the propagation of the secondary particles and the random background. Also, the simulation of the data-acquisition system of the Antares detector is described. These simulations are necessary to understand the detector response and to validate analysis techniques.

Due to the attenuation of light, the production of a detectable signal needs to be considered only in the vicinity of the detector. The simulation of the production of photons is therefore limited to a cylindrical volume around the detector, referred to as the *can*. The can extends 2.5 absorption lengths around the detector. As muons can traverse distances up to several kilometers, all processes leading to a muon have to be simulated at larger distances away from the detector. Neutrino interactions are generated in a larger volume around the detector. The size of this volume depends on the neutrino energy. The generation of neutrino events is

described in section 2.10.3.

Muons from cosmic-ray interactions are generated directly on the can using a parameterisation based on a full simulation of the cosmic-ray interaction and propagation of the subsequent shower particles. The simulation of atmospheric muons is described in section 2.10.2. A realistic background is made using real data. The random background together with the simulation of the data acquisition system is presented in section 2.10.5. A general weighting scheme, primarily used for the simulation of neutrinos is described in section 2.10.1

2.10.1 Weights

An evaluation of the detector performance involves evaluating complex multi-dimensional integrals. This can be done efficiently by means of Monte Carlo integration [57]. In Monte Carlo integration, an integral can be approximated by the uniform random sampling of N points x_i in the phase space volume V.

$$\int f dV \approx V \frac{1}{N} \sum_{i=0}^{N-1} f(x_i) \tag{2.9}$$

In general, a uniform sampling is not the best choice, because the probability density function (PDF) of the physical process under study favors certain parts of phase space. Another aspect is the optimization of the statistics within the phase space. A way to take this into account is *importance sampling* (see for example reference [58]). This generalizes formula 2.9 to the case of non-uniform sampling. This means that, when sampling according to a normalized probability density p, equation 2.9 generalizes to

$$\int f dV = \int \frac{f}{p} p dV \approx \frac{1}{N} \sum_{i=0}^{N-1} \frac{f(x_i)}{p(x_i)} \tag{2.10}$$

If an unnormalized distribution $\hat{p}$ is used, it can be normalized by dividing by V_p:

$$V_p \equiv \int \hat{p} dV \tag{2.11}$$

and thus

$$p = \frac{\hat{p}}{V_p} \tag{2.12}$$

After inserting this into equation 2.10 one obtains

$$\int f dV = \int (V_p \frac{f}{\hat{p}}) \frac{\hat{p}}{V_p} dV \approx \frac{V_p}{N} \sum_{i=0}^{N-1} \frac{f(x_i)}{\hat{p}(x_i)} \tag{2.13}$$

This result is used for the calculation of event rates. The event rate R can be calculated with :

$$R = \int P_{Earth}(E, \hat{d})\sigma(E)\rho(\vec{x})N_a\Phi(E, \hat{d})P_{det}(\vec{x}, \hat{d}, E)d\vec{x}d\Omega dE \tag{2.14}$$

where $\vec{x}$, $\hat{d}$ and E are the position of the neutrino interaction, the direction of the neutrino and the neutrino energy, respectively. The other quantities are

P_{Earth} : the probability that the neutrino reaches the detector without interacting

$\sigma(E)$: total neutrino cross section

$\rho(\vec{x})$: target density

N_a : Avogadro's number

$\Phi(E, \vec{d})$: differential neutrino flux before crossing the Earth. Typical units are number of particles per solid angle, time, area and energy (sr^{-1} s^{-1} m^{-2} GeV^{-1})

P_{det} : probability of detection

The simulated events are generated following a power-law distribution in energy, $\Phi_{gen} \propto E^{-\gamma}$. The spectral index γ is in general chosen such that the statistics at higher energies are sufficient. Normalizing the generation flux on the energy interval used for generation yields

$$\Phi_{gen} \propto \frac{E^{-\gamma}(1-\gamma)}{E_{max}^{1-\gamma} - E_{min}^{1-\gamma}} \tag{2.15}$$

Combining this with equation 2.14 according to the prescription of equation 2.13 gives :

$$\begin{aligned} R =& \frac{V 2\pi \cos(\theta_{max} - \theta_{min})(E_{max}^{1-\gamma} - E_{min}^{1-\gamma})}{(1-\gamma)N} \times \\ & \sum_{i=0}^{N-1} P_{Earth}(E_i, \hat{d}_i)\sigma(E_i)\rho(\vec{x}_i)N_a P_{det}(\vec{x}_i, \hat{d}_i, E_i)E^{\gamma}\Phi(E_i, \hat{d}_i) \end{aligned} \tag{2.16}$$

Which can be simplified to

$$R = \frac{1}{N}\sum_{i=0}^{N-1} w_i \Phi(E_i, \hat{d}_i) \tag{2.17}$$

With w_i defined as

$$\begin{aligned} w_i \equiv & \frac{1}{1-\gamma} \times \\ & V 2\pi \cos(\theta_{max} - \theta_{min})(E_{max}^{1-\gamma} - E_{min}^{1-\gamma}) \times \\ & P_{Earth}(E_i, \hat{d}_i)\sigma(E_i)\rho(\vec{x}_i)N_a P_{det}(\vec{x}_i, \hat{d}_i, E_i)E^{\gamma} \end{aligned} \tag{2.18}$$

This quantity is referred to as the weight and is calculated for each generated event. In the example given above, the event rate for a different flux can be calculated by replacing the flux in equation 2.17 by another. This removes the need to repeat the simulation when only the input flux is changed, provided that the sample contains enough statistics over the covered phase space.

2.10.2 Atmospheric muons

For the simulation of the flux of muons originating from cosmic rays, the fast simulation package MUPAGE [59] is used. MUPAGE generates atmospheric muon events at the level of the can. It is based on a parametrization of the atmospheric muon flux at the depth of the detector [60]. The parametrization is tuned on a simulation done with HEMAS [61],[62]. HEMAS simulates the primary cosmic ray interaction and propagation of the subsequent shower. The model used for the hadronic interaction is DPMJET [63]. The input to the HEMAS simulation is the primary cosmic ray flux. A phenomenological model described in [12] is used, which combines results from direct and indirect measurements of cosmic rays in an energy range from 10 GeV to 1 EeV. The propagation of muons from sea-level down to the can is simulated with the MUSIC [64] package. MUSIC takes into account energy losses due to Bremsstrahlung, pair production, inelastic scattering and knock-on electrons. It includes the distortion of the muon direction due to multiple scattering, inelastic scattering and pair production. The distributions obtained by the simulation are used to fix the parametric formulas in MUPAGE. As MUPAGE generates the events according to their abundance, no weighting of the events is needed. Each set of events corresponds to a certain observation time.

2.10.3 Neutrinos

Neutrino interactions are generated isotropically in the extended volume around the can. The size of this volume depends on the maximum neutrino energy and the zenith angle considered. The size is such that interaction products of the most energetic interactions can reach the can. The size of the generation volume is mainly determined by the muon range at the highest considered energy. For the generation of neutrino events, the Genhen [65] software package is used. The deep inelastic neutrino interactions are simulated using the LEPTO package

[66]. LEPTO integrates the differential cross sections and provides the kinematic properties of the outgoing muon. The hadronisation of the nuclear fragments is done with PYTHIA 5.7 and JETSET 7.4 [67]. The CTEQ6D parton distribution functions [33] are used. For each event, the appropriate weight is calculated (see section 2.10.1). The probability for a neutrino to reach the interaction point is included in the weight. This survival probability is calculated from the neutrino energy and the column density through the Earth associated with the neutrino direction. The calculation is done with the appropriate neutrino cross sections and takes into account the decreasing probability of a neutrino penetrating the Earth with increasing energy. If a neutrino interaction takes place within the can, all resulting particles are stored for further processing, otherwise, only the resulting muons are propagated to the can using the MUSIC package.

The most frequent neutrino signal in the Antares detector is due to atmospheric neutrinos. The atmospheric neutrino flux consists of a part due to decay of pions and kaons produced in cosmic ray interaction. In addition, there is a contribution due to the decay of charm mesons. These prompt neutrinos dominate the atmospheric neutrino flux at neutrino energies above 10^5 GeV. In this work, the atmospheric neutrino fluxes described in [68] and [69] are used.

2.10.4 Photon generation

The production of Cherenkov light is simulated within the can volume. The propagation of muons and the associated production of light is simulated using the KM3 [39] program. Within KM3, a modified version of the muon propagation code MUSIC is used. Propagation of muons is performed in steps of one meter. If the energy loss of the muon in a single step exceeds 0.3 GeV, an electromagnetic shower is generated at a random point along the path. The photon yield is extracted from pre-calculated tables in order to speed up the simulation. These tables are generated from a full simulation of a large number of muons and electro-magnetic showers with GEANT3 [70]. Measured properties of the water at the Antares site are used to simulate effects due to absorption, scattering and dispersion of the photons. The properties of the optical module are used to determine the number of detected photons. These properties include the wavelength dependent quantum efficiency and absorption in glass and gel and the angular dependence of the acceptance of the PMT.

When a neutrino interaction occurs within the can volume, the propagation of the secondary particles, excluding muons, is done with the GEASIM software package [71]. GEASIM is based on GEANT3 and performs full tracking of the particles and relevant physics processes, however, the scattering of photons is not simulated. The response of the optical modules is simulated in the same way as in KM3.

2.10.5 Simulation chain

As described in section 2.6.3, the off-shore DAQ processes supply the DataFilter process with data in a continuous stream. The simulation provides data on an event by event basis. Therefore, a dedicated software chain simulates detector operation and data taking. The chain for processing the simulated events is shown schematically in figure 2.12. A schematic view of the real data flow is also shown. The *MonteCarloEventWriter* program translates ASCII formatted output files of the physics simulation into ROOT formatted files, for efficient storage and processing. The *TriggerEfficiency* program performs the following tasks :

Electronics and PMT simulation The hits from the physics simulation are encoded in a similar way as the off-shore processes do. This includes translating the time to timestamp and TVC data and the amplitude to AVC data. This includes the effect of the ARS integration gate of 45 ns, the dead-time of 200 ns, a TTS of 1.5 ns and a typical gain spread of 30% for single photoelectrons.

Background As described in section 2.6.3 the on-line DAQ processes record the total number of L0 hits and store the data in SummaryTimeSlices. These data can be used to reproduce the uncorrelated background according to the actual conditions of a data-taking run. The data are transformed to Monte-Carlo compatible information using the program *SummaryTimeSliceWriter*. The background for a 12-line detector can be simulated using data from Line 1. The TriggerEfficiency program generates hits for each data frame according to a flat background with a rate corresponding to a randomly picked SummaryTimeSlice. These hits are then added to the data from the physics simulation.

Triggering Any of the trigger algorithms which are used in the DAQ system can be applied to the simulated data. The algorithms are identical for measured and simulated data as they share the same code. When a trigger is found, a PhysicsEvent is written to disk, together with the corresponding SummaryTimeSlice.

Writing of Data When an event is triggered, the resulting PhysicsEvent is written to disc, together with a SummaryTimeSlice and the Monte-Carlo truth information, stored in the *Event* class. Optionally, the truth information can also be written to disc even if there is no trigger.

The end-product of this chain are files that are similar to the ones produced by the DAQ system. This facilitates the use of the same programs for further analysis of the data and comparisons with the Monte-Carlo data.

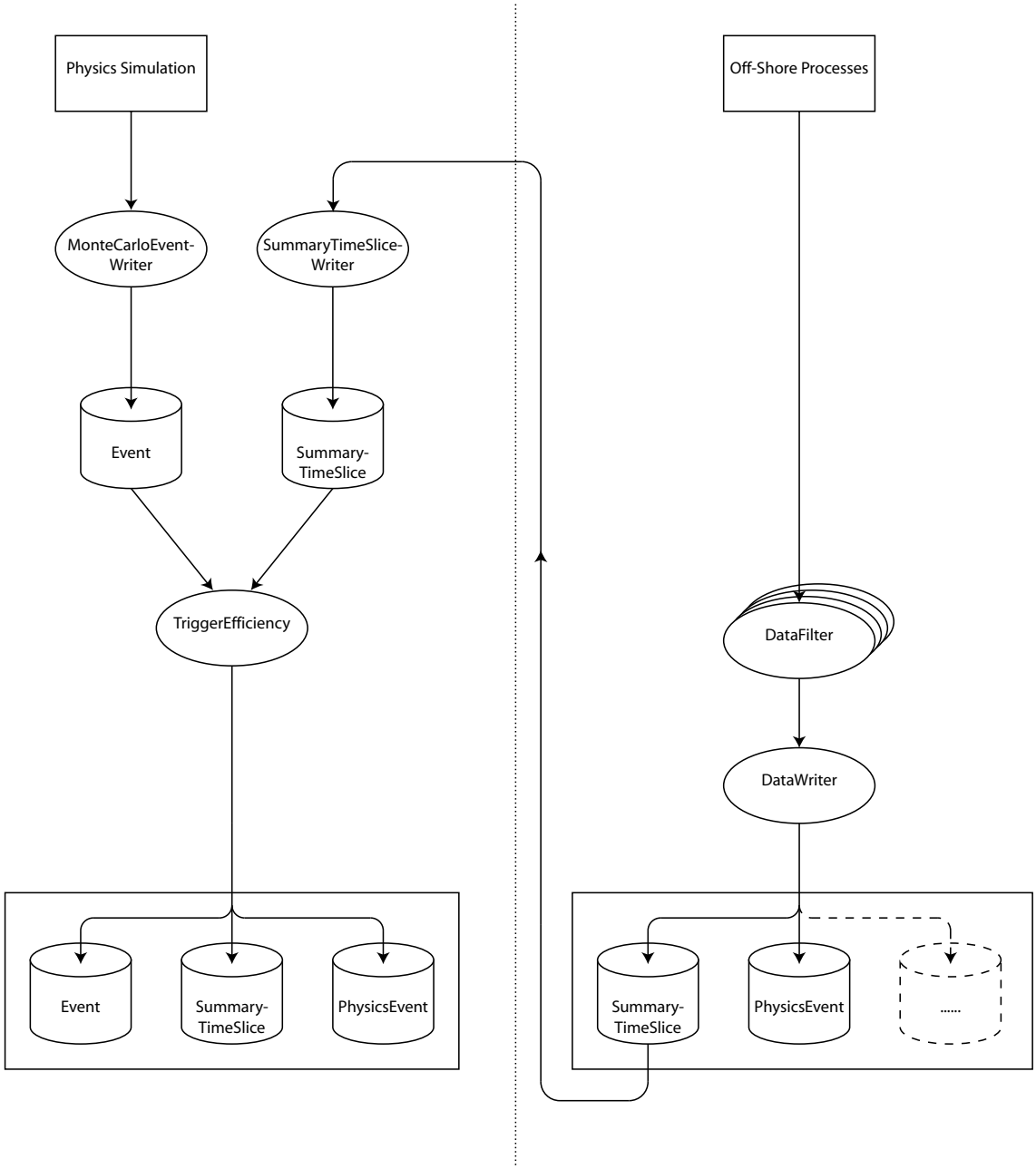

Figure 2.12: *Schematic view of the flow of data through the chain of simulation programs (left) and data (right). SummaryTimeSlices from data are used to generate the random background in the simulation.*

2.10.6 Analysis

The PhysicsEvents contain the raw ARS hit data. The TVC, timestamp and AVC values together with the logical identifiers of the ARSs can be converted to units which are directly used in the analysis. The conversion of the raw units involves

applying the calibration. Routines to make the conversion are available in the Antares DAQ software [72] which includes a common interface for both simulated and real detector geometries, including all calibration constants. The evaluation of the reconstruction algorithm in this work, and the analysis of data are done with stand-alone programs, using the available routines. A version of the reconstruction algorithm is also implemented in the Antares reconstruction and analysis framework [73] which was under development at time of writing of this thesis.